Nonlinear Koopman Modes and Coherency Identification of Coupled Swing Dynamics

Yoshihiko Susuki, *Member, IEEE* and Igor Mezić, *Member, IEEE*

***Abstract*—We perform modal analysis of short-term swing dynamics in multi-machine power systems. The analysis is based on the so-called Koopman operator, a linear, infinite-dimensional operator that is defined for any nonlinear dynamical system and captures full information of the system. Modes derived through spectral analysis of the Koopman operator, called Koopman modes, provide a nonlinear extension of linear oscillatory modes. Computation of the Koopman modes extracts single-frequency, spatial modes embedded in non-stationary data of short-term, nonlinear swing dynamics, and it provides a novel technique for identification of coherent swings and machines.**

***Index Terms*—power system, nonlinear oscillation, Koopman mode, transient stability, coherency, Koopman operator**

I. Introduction

POWER SYSTEMS exhibit complex phenomena that occur on a wide range of scales in both space and time. Examples of such phenomena contain synchronization of individual rotating machines, voltage dynamics and collapse, and cascading failures leading to widespread blackouts. Direct numerical simulations of nonlinear mathematical models have demonstrated such complex phenomena, for example, sustained oscillation [1], interarea oscillation [2], chaotic oscillation [3], and cascading failures [4]. Due to high-dimensional, spatiotemporal nature of such phenomena, it is of basic interest for practitioners to identify a small number of dominant components or *modes* that approximates the phenomena observed practically and numerically. One notion of mode developed in power system analysis is based on small-signal dynamics in which we investigate linearized equations around equilibria. However, since the phenomena listed above do not happen in the neighborhood of equilibria, it is questionable whether global modes for a linearized system are effective for describing such phenomena. Thus, there is a need to develop an alternative approach to identification of modes that does not rely on linearization. In [5] the authors used the Hilbert spectral analysis to identify a finite number of time-varying modes from a scalar data obtained with transient stability analysis. In [6] the authors used the Proper Orthonormal Decomposition (POD) to identify a set of dominant components, called PO Modes (POMs), from spatiotemporal dynamics arising in cascading failures, and in [7] the authors extracted POMs from a set of data obtained with wide-area measurement.

One of the important applications of mode identification is *coherency identification* in which for transient stability analysis one finds a group of synchronous generators swinging together with the in-phase motion. Objectives of coherency identification include development of reduced-order models and external equivalents, traditionally used to reduce computational effort and currently employ on-line dynamic security assessment, and dynamical system analysis of power system instabilities (see [8], [9]). Many groups of researchers have developed methods for coherency identification. In [10] the author used time domain simulation of linearized power system models for coherent analysis of generators subject to a disturbance. In [2], [11], [12], the authors applied time-scale separation, which was used for singular perturbation studies, to power system models and introduced the notion of slow coherency that was not dependent on any disturbances. In [12]–[15] the authors developed grouping algorithms using the slow coherency, that is, algorithms for partitioning a power system into groups of coherent generators. In [16]–[18] the authors studied the coherency using linear systems theory and decentralized systems theory such as the idea of weak coupling. In [19], [20], the authors used the energy function to identify coherent generators. In [21] the authors applied the principal component analysis to the identification of coherent generators.

In this paper, we develop an alternative method for identification of modes and coherency, by analysis of short-term swing dynamics in multi-machine power systems. Koopman pioneered the use of linear transformations on Hilbert space to analyze (nonlinear) Hamiltonian systems by introducing the so-called *Koopman operator* and studying its spectrum [22]: see [23], [24] for details. This linear, infinite-dimensional operator is defined for any nonlinear dynamical systems [23], [24]. Even if the governing dynamics of a system are finite-dimensional, the Koopman operator is infinite-dimensional and does not rely on linearization: indeed, it captures the full information of the nonlinear dynamical system. In [25] the authors identified a relationship between generalized Fourier analysis [26] and eigenfunctions of the Koopman operator. In [27] the author showed via spectral analysis of the Koopman operator that single-frequency modes can be embedded in highly nonlinear, spatiotemporal dynamics. These modes are later named the *Koopman Modes* (KMs) [28]. In [28] the authors presented a technique for characterizing the global

This work is supported in part by the JSPS Postdoctoral Fellowships for Research Abroad and in part by the NICT Project ICE-IT (Integrated Technology of Information, Communications, and Energy).

Y. Susuki is with the Department of Mechanical Engineering at the University of California, Santa Barbara, CA 93106-5070 USA, and also with the Department of Electrical Engineering at Kyoto University, Katsura, Nishikyo, Kyoto 615-8510, Japan (e-mail: susuki@ieee.org).

I. Mezić is with the Department of Mechanical Engineering at the University of California, Santa Barbara, CA 93106-5070 USA (e-mail: mezic@engineering.ucsb.edu).

behavior of complex fluid flows by decomposing a flow profile into KMs. In this paper, we apply the technique developed in [27], [28] to short-term swing dynamics in the New England 39-bus test system (NE system) [29] and the IEEE Reliability Test System-1996 (RTS-96) [30]. The NE system has 10 synchronous generators (one of which is assumed to be the infinite bus) and exhibits coupled swing dynamics. The RTS-96 includes 73 buses and 99 synchronous machines (33 generation buses, one of which is assumed to be the infinite bus). The contributions of this paper are two. We show that (i) the KM analysis identifies single-frequency, spatial modes embedded in coupled swing dynamics, and that (ii) the KM analysis can be used for identification of coherent swings and machines. The identification is performed on finite-time data of the dynamics and does not require the direct check of spatiotemporal patterns. Computation of the KMs is applicable to dynamics of any power system and can be performed purely on finite-time data of the dynamics. Thus, the identification of modes and coherency based on the KM is suitable for analysis of not only simulation outputs but also data measured in practice, for example, by wide-area measurement [31]. This paper is a substantially-enhanced version of the conference paper [32].

This paper is organized as follows. Sec. II reviews the theory of the Koopman operator, and gives the definition of KM and an algorithm for computing it from finite-time data. The definition of coherency in the context of KM is also given. Secs. III and IV analyze short-term swing dynamics of the NE system and the RTS-96, and we illustrate the effectiveness of KM analysis in identifying swings and machines. Sec. V concludes this paper with a summary and remarks.

II. Spectral Analysis Based on the Koopman Operator

We provide an introduction to the theory of the Koopman operator for nonlinear dynamical systems. The contents in Secs. II-A and II-B are based on [25], [27], [28]. The definitions of the Koopman operator and the Koopman Mode (KM) are presented. An algorithm for computation of the KM based on finite data is also presented. Finally we give the definition of coherency in the context of KM.

A. The Koopman Operator, Eigenvalue, and Mode

Consider a discrete-time, nonlinear dynamical system given by

$$\boldsymbol{x}_{k+1} \quad = \quad \boldsymbol{F}(\boldsymbol{x}_{\boldsymbol{k}}), \tag{1}$$

where $\boldsymbol{x} \in M$ is the state variable belonging to state space M, and $\boldsymbol{F} : M \to M$ is a nonlinear, vector-valued function. The *Koopman operator* is a linear operator $\mathcal{U}$ that acts on scalar-valued functions on M in the following manner: for $g : M \to \mathbb{R}$, $\mathcal{U}$ maps g into a new function $\mathcal{U}g$ given by

$$\mathcal{U}g(\boldsymbol{x}) \quad = \quad g(\boldsymbol{F}(\boldsymbol{x})).$$

Although the dynamical system is nonlinear and evolves on a finite-dimensional space, the Koopman operator $\mathcal{U}$ is linear, but infinite-dimensional. The eigenfunctions and eigenvalues of $\mathcal{U}$ are defined as follows: for functions $\varphi_j : M \to \mathbb{C}$ and constants $\lambda_j \in \mathbb{C}$,

$$\mathcal{U}\varphi_j(\boldsymbol{x}) \quad = \quad \lambda_j \varphi_j(\boldsymbol{x}), \quad j = 1, 2, \ldots$$

We refer to φ_j as *Koopman eigenfunctions* and to λ_j as the associated *Koopman eigenvalues* (KEs).

The idea in [27] is to analyze nonlinear dynamics governed by (1), using the (linear) Koopman operator $\mathcal{U}$, the Koopman eigenfunctions and eigenvalues. To this end, consider a vector-valued *observable* $\boldsymbol{g} : M \to \mathbb{R}^p$. For example, if $\boldsymbol{x} \in M$ contains the full information about system dynamics at a particular time, $\boldsymbol{g}(\boldsymbol{x})$ is a vector of any measured quantities of interest, such as frequencies and voltages measured at various points in a power system. In [27] the author shows that if the dynamical system (1) possesses a smooth invariant measure, or the initial condition $\boldsymbol{x}_0$ of (1) is on any attractor, then $\boldsymbol{g}(\boldsymbol{x}_k) = (g_1(\boldsymbol{x}_k), \ldots, g_p(\boldsymbol{x}_k))^{\mathrm{T}}$ is exactly represented as follows:

$$\boldsymbol{g}(\boldsymbol{x}_k) = \sum_{j=1}^{\infty} \lambda_j^k \varphi_j(\boldsymbol{x}_0)\boldsymbol{v}_j + \begin{bmatrix} \int_0^{2\pi} \mathrm{e}^{\mathrm{i}k\theta} \mathrm{d}E(\theta) g_1(\boldsymbol{x}_0) \\ \vdots \\ \int_0^{2\pi} \mathrm{e}^{\mathrm{i}k\theta} \mathrm{d}E(\theta) g_p(\boldsymbol{x}_0) \end{bmatrix}, \tag{2}$$

where $E(\theta)$ is a continuous, complex spectral measure. The modulus of KEs λ_i is identically one, because $\mathcal{U}$ is a unitary operator in the above situation. In (2) we refer to the vectors $\boldsymbol{v}_j$ as *Koopman Modes* (KMs) of the system (1), corresponding to $\boldsymbol{g}$. On the right-hand side of (2), the first term represents the contribution of KEs (namely, discrete spectra of $\mathcal{U}$) to the time evolution $\{\boldsymbol{g}(\boldsymbol{x}_k)\}$ and describes the average and quasi-periodic parts of $\{\boldsymbol{g}(\boldsymbol{x}_k)\}$. On the other hand, the last term represents the contribution of continuous spectrum of $\mathcal{U}$ and describes the aperiodic part of $\{\boldsymbol{g}(\boldsymbol{x}_k)\}$. Hence, if the dynamics observed in (1) have no continuous spectrum in frequency domain (practical experience suggests this situation in power system analysis), then the dynamics are exactly represented as

$$\boldsymbol{g}(\boldsymbol{x}_k) \quad = \quad \sum_{j=1}^{\infty} \lambda_j^k \varphi_j(\boldsymbol{x}_0)\boldsymbol{v}_j. \tag{3}$$

In [25], [27], the authors show that the terms $\varphi_j(\boldsymbol{x}_0)\boldsymbol{v}_j$ are defined and computed with a projection operation associated with $\mathcal{U}$ applied to the observable $\boldsymbol{g}$. Define a family of operators $\mathcal{P}^\nu$: for $g : M \to \mathbb{R}$,

$$\mathcal{P}^\nu g(\boldsymbol{x}_0) \quad = \quad \lim_{n\to\infty} \frac{1}{n} \sum_{k=0}^{n-1} \mathrm{e}^{-\mathrm{i}2\pi k\nu} g(\boldsymbol{x}_k),$$

where $\nu \in [-1/2, 1/2)$. When the initial condition $\boldsymbol{x}_0$ is on an attractor of (1), a nonzero $\mathcal{P}^\nu$ is the orthogonal projection operator onto the eigenspace of $\mathcal{U}$ associated with the KE $\lambda = \mathrm{e}^{\mathrm{i}2\pi\nu}$. The projections of the p components $g_1, \ldots, g_p$ of $\boldsymbol{g}$ on the j-th eigenspace are obtained:

$$\begin{bmatrix} \mathcal{P}^{\nu_j} g_1(\boldsymbol{x}_0) \\ \vdots \\ \mathcal{P}^{\nu_j} g_p(\boldsymbol{x}_0) \end{bmatrix} \quad = \quad \varphi_j(\boldsymbol{x}_0)\boldsymbol{v}_j, \tag{4}$$

where $\nu_j = \mathrm{Im}[\ln \lambda_j]/2\pi$. This formula (4) associates $\varphi_j(\boldsymbol{x}_0)\boldsymbol{v}_j$ with the projection operation based on the operator $\mathcal{P}^\nu$. The left-hand sides of (4) are just the Fourier transforms of observations $\{\boldsymbol{g}(\boldsymbol{x}_0), \boldsymbol{g}(\boldsymbol{x}_1), \ldots\}$, and the terms $\varphi_j(\boldsymbol{x}_0)\boldsymbol{v}_j$ can be easily computed.

Here we have assumed that the dynamics of (1) are on an attractor. Even if this is not the case, that is, we consider dynamics off attractors of (1), the KM modes oscillate with a single frequency. If each of the p components of $\boldsymbol{g}$ lies within the span of eigenfunctions φ_j, then, as in [28], we may expand the vector-valued $\boldsymbol{g}$ in terms of these eigenfunctions as

$$\boldsymbol{g}(\boldsymbol{x}) \;=\; \sum_{j=1}^{\infty} \varphi_j(\boldsymbol{x})\boldsymbol{w}_j,$$

where $\boldsymbol{w}_j$ are regarded as the (vector) coefficients in the expansion. The time evolution $\{\boldsymbol{g}(\boldsymbol{x}_k)\}$ starting at $\boldsymbol{g}(\boldsymbol{x}_0)$ is identically given by (3):

$$\begin{aligned}\boldsymbol{g}(\boldsymbol{x}_k) &= \sum_{j=1}^{\infty} \varphi_j(\boldsymbol{x}_k)\boldsymbol{w}_j \;=\; \sum_{j=1}^{\infty} \mathcal{U}^k \varphi_j(\boldsymbol{x}_0)\boldsymbol{w}_j \\ &= \sum_{j=1}^{\infty} \lambda_j^k \varphi_j(\boldsymbol{x}_0)\boldsymbol{w}_j.\end{aligned}$$

Thus we can refer to $\boldsymbol{w}_j$ as the KM which oscillates with a single frequency. If the dynamics observed here have only a finite number of discrete spectra in frequency domain, then we can expect the expansion gives a good approximation of the dynamics. For dynamics off attractors, the KE λ_j therefore characterizes the temporal behavior of the corresponding KM $\boldsymbol{w}_j$: the phase of λ_j determines its frequency, and the magnitude determines the growth rate.

B. Computation of the Koopman Eigenvalues and Modes

While the general Fourier analysis allows us to compute KMs on an attractor, off attractors the KMs as well as KEs can be computed using the Arnoldi algorithm [28]. Suppose that we have a sequence of $N+1$ observations $\{\boldsymbol{g}(\boldsymbol{x}_0), \ldots, \boldsymbol{g}(\boldsymbol{x}_N)\}$. Let us define the *empirical Ritz values* $\tilde{\lambda}_j$ and *empirical Ritz vectors* $\tilde{\boldsymbol{v}}_j$ of this sequence by using the following algorithm:

(i) Define constants c_j such that for vector $\boldsymbol{r}$ satisfying $\boldsymbol{r} \perp \mathrm{span}\{\boldsymbol{g}(\boldsymbol{x}_0), \ldots, \boldsymbol{g}(\boldsymbol{x}_{N-1})\}$,

$$\boldsymbol{r} \;=\; \boldsymbol{g}(\boldsymbol{x}_N) - \sum_{j=0}^{N-1} c_j \boldsymbol{g}(\boldsymbol{x}_j). \tag{5}$$

(ii) Define the companion matrix C as

$$\mathsf{C} \;=\; \begin{bmatrix} 0 & 0 & \cdots & 0 & c_0 \\ 1 & 0 & \cdots & 0 & c_1 \\ 0 & 1 & \cdots & 0 & c_2 \\ \vdots & \vdots & \ddots & \vdots & \vdots \\ 0 & 0 & \cdots & 1 & c_{N-1} \end{bmatrix}.$$

and find its N eigenvalues $\tilde{\lambda}_1, \ldots, \tilde{\lambda}_N$.

(iii) Define the Vandermonde matrix T using $\tilde{\lambda}_j$ as

$$\mathsf{T} \;=\; \begin{bmatrix} 1 & \tilde{\lambda}_1 & \tilde{\lambda}_1^2 & \cdots & \tilde{\lambda}_1^{N-1} \\ 1 & \tilde{\lambda}_2 & \tilde{\lambda}_2^2 & \cdots & \tilde{\lambda}_2^{N-1} \\ \vdots & \vdots & \vdots & \ddots & \vdots \\ 1 & \tilde{\lambda}_N & \tilde{\lambda}_N^2 & \cdots & \tilde{\lambda}_N^{N-1} \end{bmatrix}.$$

(iv) Define $\tilde{\boldsymbol{v}}_j$ to be the columns of $\mathsf{V} = [\boldsymbol{g}(\boldsymbol{x}_0)\, \boldsymbol{g}(\boldsymbol{x}_1) \cdots \boldsymbol{g}(\boldsymbol{x}_{N-1})]\mathsf{T}^{-1}$.

Then, we have the following equations that are originally derived in [28]:

$$\boldsymbol{g}(\boldsymbol{x}_k) = \sum_{j=1}^{N} \tilde{\lambda}_j^k \tilde{\boldsymbol{v}}_j, \quad \boldsymbol{g}(\boldsymbol{x}_N) = \sum_{j=1}^{N} \tilde{\lambda}_j^N \tilde{\boldsymbol{v}}_j + \boldsymbol{r}, \tag{6}$$

where $k = 0, \ldots, N-1$. Comparing with (3), the empirical Ritz values $\tilde{\lambda}_j$ and vectors $\tilde{\boldsymbol{v}}_j$ behave precisely in the same manner as the KEs λ_i and the terms $\varphi_i(\boldsymbol{x}_0)\boldsymbol{v}_i$ of Koopman eigenfunctions and KMs, but for the finite sum (6) instead of the infinite sum (3).

C. Coherency in the Koopman Mode

Finally, we define the notion of coherency in the context of KM. The case of oscillatory KM, in which the KE has an imaginary part, is addressed, because the study on coherency identification in power systems normally deals with oscillatory responses following a disturbance. For an oscillatory KM $\boldsymbol{v}_j$, called Mode j, with the KE $\lambda_j = r_j \mathrm{e}^{\mathrm{i}2\pi\nu_j}$ and its complex conjugate $\lambda_j^{\mathrm{c}} = r_j \mathrm{e}^{-\mathrm{i}2\pi\nu_j}$, the corresponding modal dynamics, denoted by $\boldsymbol{g}^j(\boldsymbol{x}_k)$, are given by

$$\begin{aligned}\boldsymbol{g}^j(\boldsymbol{x}_k) &= \lambda_j^k \varphi_j(\boldsymbol{x}_0)\boldsymbol{v}_j + (\lambda_j^{\mathrm{c}})^k \{\varphi_j(\boldsymbol{x}_0)\boldsymbol{v}_j\}^{\mathrm{c}} \\ &= 2r_j^k \begin{bmatrix} A_{j1}\cos(2\pi k\nu_j + \alpha_{j1}) \\ \vdots \\ A_{jp}\cos(2\pi k\nu_j + \alpha_{jp}) \end{bmatrix},\end{aligned} \tag{7}$$

where

$$\left.\begin{aligned} A_{ji} &= \sqrt{(\mathrm{Re}[\varphi_j(\boldsymbol{x}_0)\boldsymbol{v}_j]_i)^2 + (\mathrm{Im}[\varphi_j(\boldsymbol{x}_0)\boldsymbol{v}_j]_i)^2}, \\ \tan\alpha_{ji} &= \frac{\mathrm{Im}[\varphi_j(\boldsymbol{x}_0)\boldsymbol{v}_j]_i}{\mathrm{Re}[\varphi_j(\boldsymbol{x}_0)\boldsymbol{v}_j]_i}. \end{aligned}\right\}$$

The notation $\mathrm{Re}[\varphi_j(\boldsymbol{x}_0)\boldsymbol{v}_j]_i$ stands for the i-th component of vector $\mathrm{Re}[\varphi_j(\boldsymbol{x}_0)\boldsymbol{v}_j]$. The real part of $\varphi_j(\boldsymbol{x}_0)\boldsymbol{v}_j$ determines the initial *amplitude* of modal dynamics, and the imaginary part affects their initial *phase*. Thus, we can say that a set of oscillatory components $\mathbb{I} \subseteq \{1, \ldots, p\}$ is *coherent* with respect to Mode j if the amplitude coefficients A_{ji} are the same for all $i \in \mathbb{I}$, and the initial phases α_{ji} are also the same[1]. Then, for coherent identification for Mode j, it is sufficient to check both the amplitude coefficients A_{ji} and initial phases α_{ji}. Numerically, it is enough to group oscillatory components with similar amplitude coefficient A_{ji} and initial phase α_{ji} as a set of coherent components. When the observations $\{\boldsymbol{g}(\boldsymbol{x}_k)\}$ contain swing dynamics of synchronous machines in a power system, we can find a coherent group of the machines in which they swing together in frequency and phase.

[1]The definition is strict compared with the definitions of slow-coherency [2], [11] and near-coherency [16], because it does not admit any finite, constant phase difference of swings. It is easily relaxed and can match the definitions of coherency proposed previously.

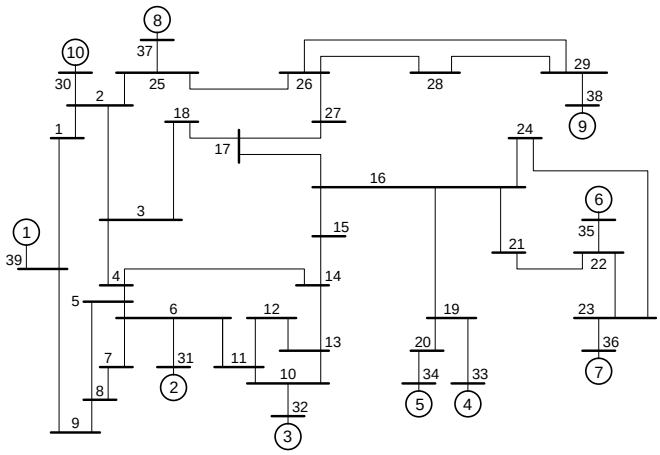

Fig. 1. The New England 39-bus test system (NE system) [29]

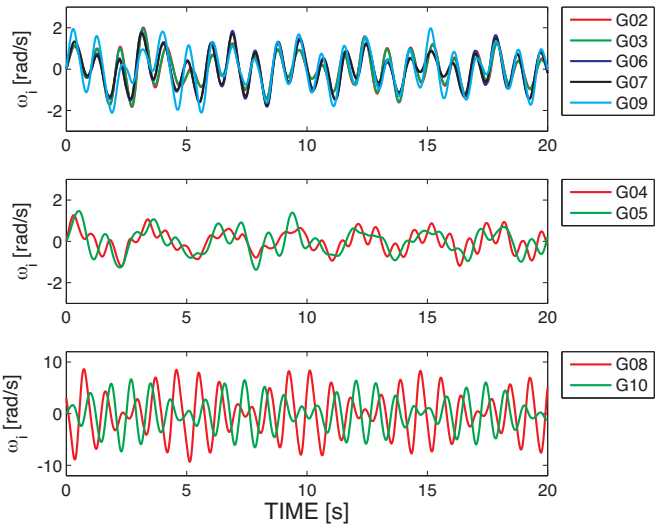

Fig. 2. Coupled swing dynamics of generators 2–10 in the New England test system. These are the trajectories of (8) for the initial condition (9).

III. Application to the New England Test System

We apply the above-described computation of Koopman mode to analyze short-term swing dynamics in the New England 39-bus test system (NE system). The NE system is shown in Fig. 1 and contains the 10 generation units (equivalent 10 synchronous generators, circled numbers in the figure), the 39 buses, and AC transmission lines. Most of the buses have constant active and reactive power loads. The details of the system, such as unit rating, line data, and loading conditions, are given in [29]. The purpose of the application is to show that the KM analysis can be used for identification of coherent swings and generators in a test system.

A. The Classical Model

First, we introduce the equations of motion of generators in the NE system. Assume that bus 39 is the infinite bus. The short-term swing dynamics of generators 2–10 are represented by the following nonlinear differential equations, the so-called classical model [33]:

$$\left.\begin{aligned} \frac{\mathrm{d}\delta_i}{\mathrm{d}t} &= \omega_i, \\ \frac{H_i}{\pi f_\mathrm{b}}\frac{\mathrm{d}\omega_i}{\mathrm{d}t} &= -D_i\omega_i + P_{\mathrm{m}i} - G_{ii}E_i^2 \\ &\quad - \sum_{j=1,j\neq i}^{10} E_iE_j\left\{G_{ij}\cos(\delta_i-\delta_j) + B_{ij}\sin(\delta_i-\delta_j)\right\}, \end{aligned}\right\} \quad (8)$$

where the integer label $i = 2, \ldots, 10$ denotes generator i. The variable δ_i is the angular position of rotor in generator i with respect to bus 1 and is in radians [rad]. The variable ω_i is the deviation of rotor speed in generator i relative to that of bus 1 and is in radians per second [rad/s]. We set the variable δ_1 to a constant, because bus 39 is assumed to be the infinite bus. The parameters f_b, H_i, D_i, $P_{\mathrm{m}i}$, E_i, G_{ii}, G_{ij}, and B_{ij} are in per unit system except for H_i and D_i in seconds [s], and for f_b in Hertz [Hz]. The mechanical input power $P_{\mathrm{m}i}$ to generator i and the internal voltage E_i of generator i are normally constant in the short-term regime [33]. The parameter H_i is the per unit time inertia constant of generator i, and D_i its damping coefficient. The parameter G_{ii} is the internal conductance, and $G_{ij} + \mathrm{j}B_{ij}$ is the transfer impedance between generators i and j. Electrical loads are modeled as passive impedances. Note that any model of exciter is not included in the current model. We have a simulation output of dynamics in the NE system using a detailed model with exciter. In the simulation output, electromechanical dynamics and modes are dominant which we study in this paper.

B. Numerical Simulation of the Classical Model

The setting of numerical simulation is as follows. The voltage E_i and a stable equilibrium $(\delta_i^*, \omega_i^* = 0)$ for generator i are fixed using power flow computation [33]. The constants H_i, $P_{\mathrm{m}i}$, and power loads are the same as in [29]. The parameter D_i is fixed at 0.005 s, and f_b at 50 Hz. The elements G_{ii}, G_{ij}, and B_{ij} are calculated using the data in [29] and the power flow computation. All numerical simulations discussed in this paper were performed using MATLAB: the function `ode45` is adopted for numerical integration of (8).

We present an example of short-term swing dynamics in the NE system. Fig. 2 shows the time responses of rotor speed deviations ω_i under the initial condition:

$$(\delta_i(0), \omega_i(0)) = \begin{cases} (\delta_i^* + 1.5\,\mathrm{rad}, 3\ \mathrm{rad/s}) & i = 8, \\ (\delta_i^*, 0\,\mathrm{rad/s}) & \text{else.} \end{cases} \quad (9)$$

The initial condition physically corresponds to a local disturbance at generator 8. A more natural disturbance is used in Sec. IV for analysis of the IEEE Reliability Test System-1996. The generators do not show any stepping-out in the figure, that is, they do not show any loss of transient stability for the selected disturbance. Generators 2, 3, 6, and 7 show a coherent swing excited by the local disturbance. Note that the current way of selecting coherent generators is heuristic, i.e., by checking their swing forms. We call these generators the coherent group. The other generators show incoherent swings in the figure. Generator 9 shows a swing similar in frequency

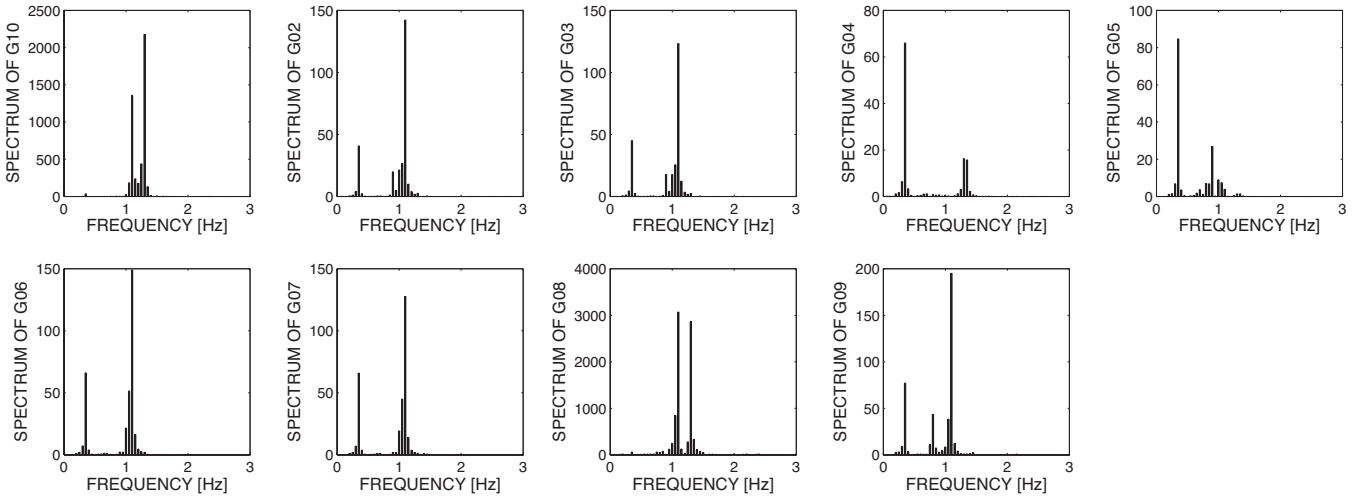

Fig. 3. Numerical discrete Fourier transform of time responses shown in Fig. 2

and phase to the coherent group, but the swing amplitude is a little larger. Generators 8 and 10 have swings of larger amplitudes than the others, because the initial condition is localized at generator 8, and the two generators are electrically close. Fig. 3 shows the Discrete Fourier Transform (DFT) of the time responses shown in Fig. 2. The computation is done by the function `fft` in MATLAB, and the sampling frequency is 50 Hz. The DFT results on generators 8 and 10 have larger magnitudes than the others and have the same shape with two peaks (1.10 Hz and 1.30 Hz). The coherent group—generators 2, 3, 6, and 7—has the same shape with two peaks (0.35 Hz and 1.10 Hz). Since DFT does not consider phase information, we cannot conclude from the DFT results that generators 2, 3, 6, and 7 swing coherently. The shape for generator 9 has three peaks (0.35 Hz, 0.80 Hz, and 1.10 Hz) and hence produces a swing similar to that of the coherent group. The other generators, 4 and 5, have shapes different from those mentioned previously.

C. Koopman Modes and Eigenvalues for the Simulation Output

We compute the Koopman Modes (KMs) and Koopman eigenvalues (KEs) for the coupled swing dynamics shown in Fig. 2. The computation is done with the two different algorithms. One is based on the Fourier-based formula (4), and the other is the Arnoldi-based algorithm introduced in Sec. II-B. For computation we need to choose the observable $\boldsymbol{g}(\boldsymbol{\delta}, \boldsymbol{\omega})$ where $\boldsymbol{\delta} = (\delta_2, \ldots, \delta_{10})^{\mathrm{T}}$ and $\boldsymbol{\omega} = (\omega_2, \ldots, \omega_{10})^{\mathrm{T}}$. The symbol T indicates (complex conjugate) transpose in vectors. In this paper we use the variables of rotor speed deviations, $\boldsymbol{\omega}$, as the observable: $\boldsymbol{g}(\boldsymbol{\delta}, \boldsymbol{\omega}) = \boldsymbol{\omega}$. This observable has a clear physical meaning in power systems: one measures rotor speeds or frequencies for every generation plant. We use the simulation output shown in Fig. 2 that extracts $\{\boldsymbol{\omega}(nT)\}_{n=0}^{N}$, where the uniform sampling period $T = 1/(50\,\mathrm{Hz})$ and the number of samples $N + 1 = 1001$.

Recall from Fig. 3 that generators 2, 3, 6, and 7 have the similar shape of spectrum with peak frequencies 0.35 Hz and 1.10 Hz, and that generators 8 and 10 have the peak frequencies 1.10 Hz and 1.30 Hz. Hence we compute the terms including KMs, $\varphi_i(\boldsymbol{x}_0)\boldsymbol{v}_i$, using the projection operator $\mathcal{P}^{\nu}$ with $\nu = (0.35\,\mathrm{Hz})T$, $(1.10\,\mathrm{Hz})T$, and $(1.30\,\mathrm{Hz})T$. We use the finite-time approximation of (4) from $k = 0$ to N, where $N + 1$ is the number of samples. The numerical results are shown in Fig. 4. The amplitude coefficients and initial phases, which are defined in (7), are also shown. For 0.35 Hz, the values of amplitude coefficients are close for each of the

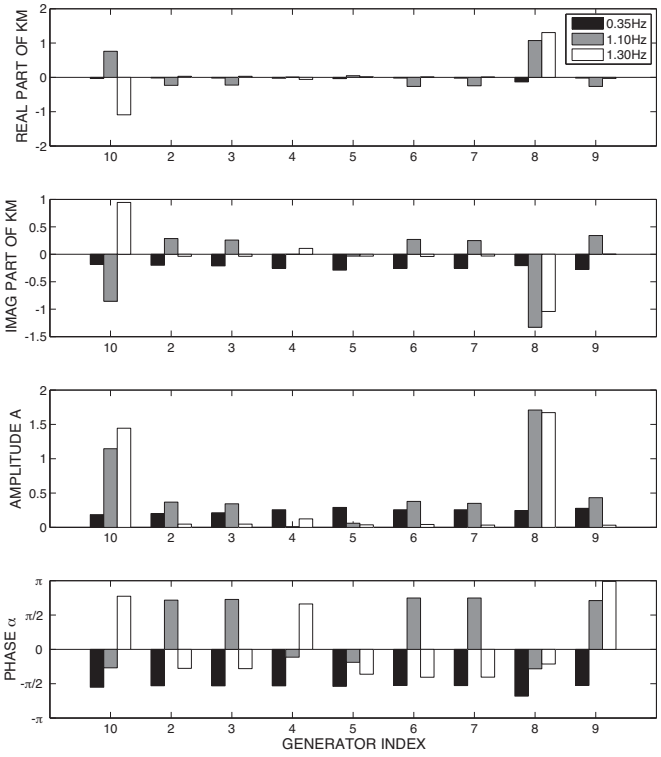

Fig. 4. Numerical results of terms $\varphi_i(\boldsymbol{x}_0)\boldsymbol{v}_i$ using the Fourier-based formula (4) under $\nu = (0.35\,\mathrm{Hz})T$, $(1.10\,\mathrm{Hz})T$, and $(1.30\,\mathrm{Hz})T$. The amplitude coefficients A_{ji} and initial phases α_{ji}, defined in (7), are shown.

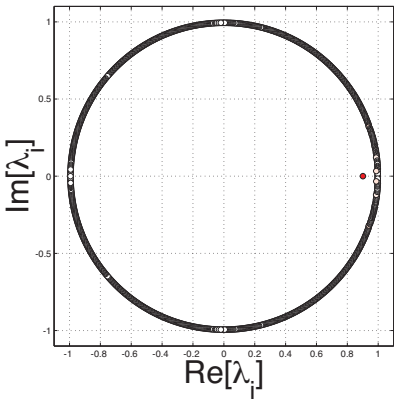

Fig. 5. The empirical Ritz values $\tilde{\lambda}_j$ obtained with the Arnoldi-based algorithm. The color varies smoothly from red to white, depending on the norm of the corresponding mode.

TABLE I
NUMERICAL RESULTS ON THE KOOPMAN MODES OBTAINED WITH THE ARNOLDI-BASED ALGORITHM

Mode j	Growth Rate $\lvert\tilde{\lambda}_j\rvert$	Argument [rad] $\tilde{\theta}_j = \mathrm{Im}[\ln \tilde{\lambda}_j]$	Frequency [Hz] $\tilde{f}_j = \lvert\tilde{\theta}_j\rvert/(2\pi T)$	Norm $\lVert\tilde{\boldsymbol{v}}_j\rVert$
1	0.9986	$\pm$0.1701	1.3533	3.0021
2	0.9986	$\pm$0.1438	1.1447	2.3930
3	0.9985	$\pm$0.1009	0.8028	0.7039
4	0.9985	$\pm$0.1300	1.0343	0.9753
5	0.9984	$\pm$0.0931	0.7405	0.4507
6	0.9984	$\pm$0.1130	0.8990	0.8162
7	0.9983	$\pm$0.1643	1.3078	6.6147
8	0.9983	$\pm$0.1378	1.0962	7.1941
9	0.9983	$\pm$0.0468	0.3727	2.1006
10	0.9982	$\pm$0.1836	1.4612	1.2238

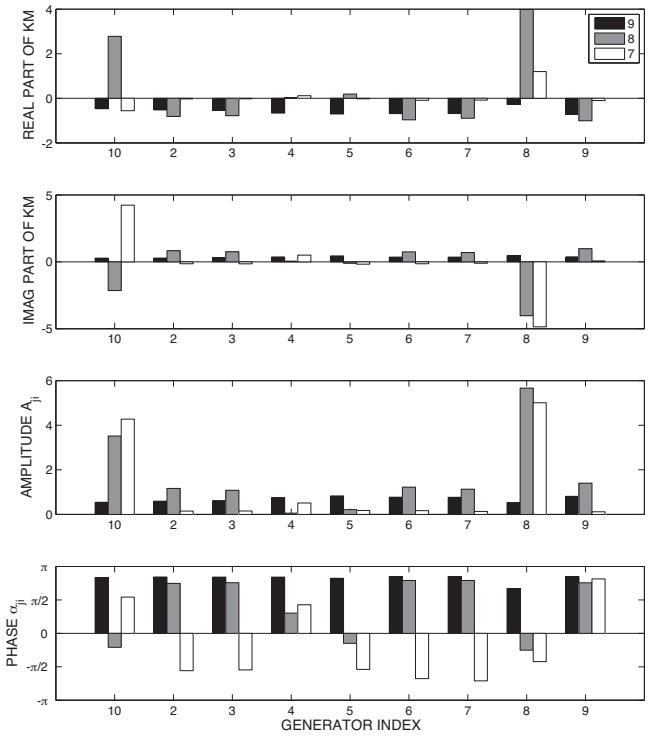

Fig. 6. The Koopman modes $\tilde{\boldsymbol{v}}_j$ ($j = 7, 8, 9$) in Tab. I. They are obtained with the Arnoldi-based algorithm. The amplitude coefficients A_{ji} ($i = 2, \ldots, 10$) and initial phases α_{ji}, defined in (7), are shown.

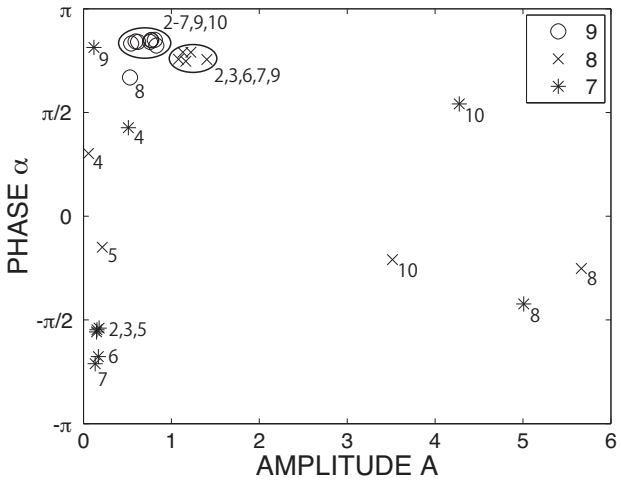

Fig. 7. Distribution of amplitude coefficients A_{ji} and initial phases α_{ji} for the Koopman modes ($j = 7, 8, 9$) shown in Fig. 6. The numbers inside the figure (e.g. 8,10) denote the integer labels of generators.

generators, and their initial phases are also close except for generator 8. Hence the generators except for 8 show in-phase swings with 0.35 Hz. For 1.10 Hz, the values of amplitude coefficients and initial phases are close for generators 2, 3, 6, 7, and 9, and hence they show in-phase swings with 1.10 Hz. The two KMs with 0.35 Hz and 1.10 Hz capture the coherent motion of generators 2, 3, 6, 7, and 9. For 1.10 Hz and 1.30 Hz, the amplitude coefficients for generators 8 and 10 are larger than the others. These two KMs capture the large swings of generators 8 and 10 observed in Fig. 2. Thus, we can extract spatial modes oscillating with a single frequency from the simulation output of the NE system.

Next we compute the KEs and KMs (the empirical Ritz values $\tilde{\lambda}_j$ and associated vectors $\tilde{\boldsymbol{v}}_j$) using the Arnoldi-based algorithm. The implementation of Step (i) in the algorithm is explained in Appendix A. Fig. 5 shows the empirical Ritz values $\tilde{\lambda}_j$. The norm of $\boldsymbol{r}$ in Steps (i) and (iii) is of order 10^{-12}. Many KMs are obtained and are close to the unit circle $|\tilde{\lambda}_j| = 1$. Now let us focus on KMs that have both large growth rates $|\tilde{\lambda}_j|$ and large norms of $\tilde{\boldsymbol{v}}_j$. Such modes represent sustained swing components for the time duration of simulation outputs and have dominant magnitudes in the outputs. Tab. I shows numerical results on KEs and KMs, which we call Mode 1 to Mode 10. The norm for Mode j is defined as $||\tilde{\boldsymbol{v}}_j|| = \sqrt{\tilde{\boldsymbol{v}}_j^{\mathrm{T}} \tilde{\boldsymbol{v}}_j}$. The order of KMs in Tab. I is based on the magnitudes of growth rates. Now we pick up Mode 7 to Mode 9 that have large norms in the table. Mode 1 and Mode 2 have large norms, too. But their frequencies are close to Mode 7 and Mode 8, respectively. Fig. 6 shows the KMs $\tilde{\boldsymbol{v}}_j$ for Mode j ($j = 7, 8, 9$). The amplitude coefficients A_{ji} ($j = 7, 8, 9, i = 2, \ldots, 10$) and initial phases α_{ji}, defined in (7), are also shown. We display the results in order to make it easy to compare this with the Fourier-based results in Fig. 4. For example, the frequency 1.3078 Hz of Mode 7 is close to one of the dominant frequencies for generators 8 and 10, that is, 1.30 Hz. In fact, since the values of amplitude coefficients $A_{7,i}$ in Fig. 6 are large for generators 8 and 10, the corresponding modal dynamics are localized at these generators. Thus, we can decompose the coupled swing dynamics in the NE system

TABLE II
EIGENVALUES OF THE LINEAR GLOBAL MODES

Mode i	Eigenvalue λ_i^*	Frequency f_i^* [Hz]
1	$-0.0128 \pm \mathrm{j}2.6558$	0.4227
2	$-0.0131 \pm \mathrm{j}8.8584$	1.4099
3	$-0.0135 \pm \mathrm{j}8.8874$	1.4145
4	$-0.0137 \pm \mathrm{j}8.5658$	1.3633
5	$-0.0128 \pm \mathrm{j}5.4512$	0.8676
6	$-0.0127 \pm \mathrm{j}5.9619$	0.9489
7	$-0.0129 \pm \mathrm{j}6.5890$	1.0487
8	$-0.0123 \pm \mathrm{j}7.4029$	1.1782
9	$-0.0119 \pm \mathrm{j}7.4457$	1.1850

into a set of KMs, namely, spatial modes of oscillation with single frequency.

The decomposition into KMs makes it possible to extract coherent generators in the coupled swing dynamics. In fact, the two KMs, Mode 8 and Mode 9, capture a coherent motion related to the coherent group of generators. These frequencies, 1.0962 Hz and 0.3727 Hz, are close to the frequencies of the coherent group, 1.10 Hz and 0.35 Hz. For Mode 8, the values of $A_{8,i}$ are close for each of generators 2, 3, 6, 7, and 9, and their initial phases $\alpha_{8,i}$ are also close. The distribution of $A_{8,i}$ and $\alpha_{8,i}$ is plotted in Fig. 7. The points ($\times$) for generators 2, 3, 6, 7, and 9 are clustered around the coordinate $(1.2, -0.7)$. Hence generators 2, 3, 6, 7, and 9 show in-phase swings with 1.0962 Hz. For Mode 9, the values of $A_{9,i}$ and $\alpha_{9,i}$ are close for each of the generators except for generator 8, and hence they show in-phase swings with 0.3727 Hz. The corresponding plots ($\circ$) in Fig. 7 are clustered except for generator 8. The two KMs capture the coherent motion of generators 2, 3, 6, 7, and 9. In this way, we can identify the coherent group observed in Fig. 2 by using the decomposition into KMs. The plot of amplitude coefficients and initial phases as Fig. 7 provides a systematic way to identify coherent swings and generators by using an automatic clustering algorithm.

In this subsection, we used the Fourier-based formula (4) and the Arnoldi algorithm in Sec. II-B to compute the KMs and KEs. The results for amplitude coefficients and initial phases between Fig. 4 and Fig. 6 with Mode 7 to Mode 9 are compared. The results for amplitude coefficients are qualitatively similar. However, the results for initial phases are somewhat different, especially at generator 8. Also, for the amplitude coefficients, there are quantitative differences between the results in Figs. 4 and 6. These differences might be due to the fact that the Fourier-based formula (4) presumes the dynamics are on an attractor. Indeed, the current analysis is performed for transient dynamics. However, identification of coherent swings and generators is possible using both the algorithms. In fact, the coherent swings of generators 2, 3, 6, 7, and 9 are captured well.

D. Comparisons with Linear Global Modes and Proper Orthonormal Modes

In this section, we compare the numerical results on KMs with conventional modes that have been used in power system analysis: Linear Global Modes (LGMs) and Proper Orthonormal Modes (POMs).

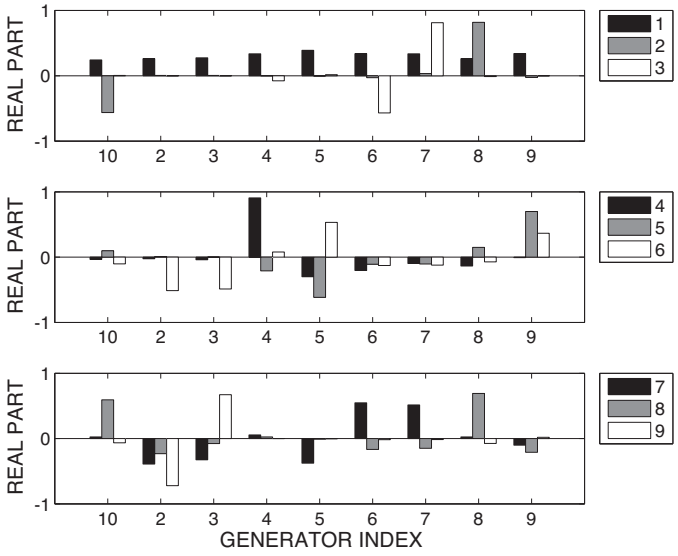

Fig. 8. The real parts of the Linear Global Modes (LGMs). These results are obtained by computing eigenvectors $\boldsymbol{v}_i^*$ of matrix A for the linearized classical model.

First, we consider the linearized dynamics around the stable equilibrium $(\delta_i^*, 0)$ of (8). The linearized system associated with (8) is represented by the constant coefficient matrix $\mathsf{A} \in \mathbb{R}^{18\times 18}$. Let $\boldsymbol{v}_i^* \in \mathbb{C}^{18}$ be eigenvectors and $\lambda_i^* \in \mathbb{C}$ be eigenvalues of A:

$$\mathsf{A}\boldsymbol{v}_i^* \quad = \quad \lambda_i^* \boldsymbol{v}_i^*, \quad i = 1, \ldots, 18.$$

Tab. II shows the eigenvalues λ_i^* and associated frequencies f_i^* of A. They are the nine independent complex conjugate pairs, and these eigenfrequencies range from 0.4 Hz to 1.5 Hz. The associated eigenvectors, namely, LGMs, are the nine independent complex conjugate pairs, and the real parts of LGMs for $\boldsymbol{\omega}$ are shown in Fig. 8.

Now we compare the LGMs with the results on KMs. The frequencies of LGM 1, LGM 8, and LGM 2 (0.4227 Hz, 1.1782 Hz, and 1.4099 Hz) are close to the frequencies used in Fig. 4 (0.35 Hz, 1.10 Hz, and 1.30 Hz). The shapes of real parts of the LGMs and the KMs are also similar. These imply that both the LGMs and the KMs can capture the coherent group. In the current simulation, since the dynamics are weakly dissipative and converge to the stable equilibrium as time passes, the results on LGMs and KMs become close. This is a natural conclusion, because KMs for a linear system coincide with LGMs [28]. However, the frequencies of LGMs are quantitatively different from the frequencies obtained with DFT. The KM results using Arnoldi-based algorithm estimate swing frequencies correctly: Mode 9 (0.3727 Hz), Mode 8 (1.0962 Hz), and Mode 7 (1.3078 Hz) in Tab. I. Thus the KMs provide a nonlinear extension of LGMs and captures swing frequencies embedded in nonlinear, coupled dynamics correctly. In particular, the KMs based on the Arnoldi algorithm provide an effective method for transient stability analysis, because it is associated with dynamics far from attractors of pre- and post-fault systems.

Next we compare the KMs with POMs. The POD provides

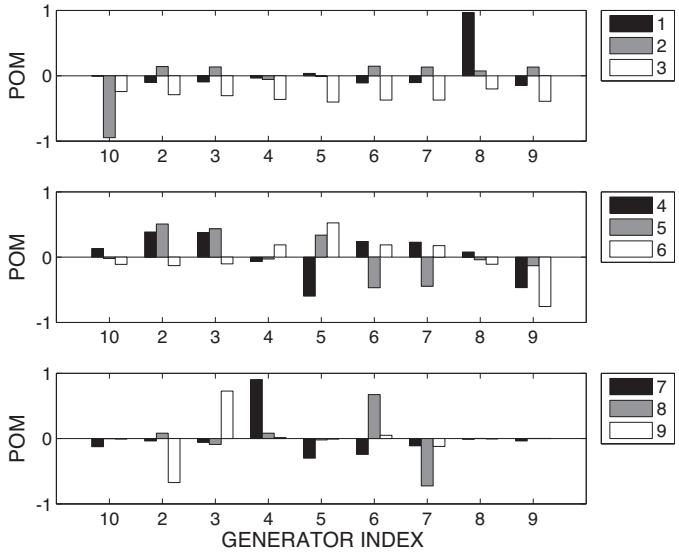

Fig. 9. Proper Orthonormal Modes (POMs) $\boldsymbol{e}_j$ for the coupled swing dynamics shown in Fig. 2. They are orthonormal eigenvectors of correlation matrix for the simulation output $\{\boldsymbol{\omega}(nT)\}$ $(n = 0, \ldots, N)$.

a basis for the modal decomposition of an ensemble of functions, such as data obtained in the course of experiments, and provides, energy-wise, the most efficient, orthogonal way of capturing the dominant components of the process [34], [35]. Consider simulation outputs of rotor speed deviations, $\{\boldsymbol{\omega}(nT)\}$ $(n = 0, \ldots, N)$. The outputs are represented by

$$\boldsymbol{\omega}(nT) \quad = \quad \sum_{j=1}^{9} \boldsymbol{e}_j a_j(nT).$$

We require the time-invariant basis vectors $\boldsymbol{e}_j$ $(j = 1, \ldots, 9)$, called POMs, to be orthonormal and closest in energy norm to the output. Every vector $\boldsymbol{e}_j$ is obtained by computing the correlation matrix R from $\{\boldsymbol{\omega}(nT)\}$ and by finding the orthonormal eigenvectors of R: see [35] for details. The time-varying coefficients a_j $(j = 1, \ldots, 9)$ hold the following correlation property: $\langle a_j a_k \rangle = \langle a_j^2 \rangle$ (if $j = k$) or 0 (otherwise), where $\langle \bullet \rangle$ denotes a time average of $\{\bullet\}$. POMs are ordered by $\langle a_j^2 \rangle \geq \langle a_{j+1}^2 \rangle$.

The POMs for our problem are presented in Figs. 9 and 10. Fig. 9 shows the POMs $\boldsymbol{e}_j$. The 1st POM has the dominant peak at generator 8, and the 2nd POM has the peak at generator 10. These modes are uniform at the coherent group, i.e. generators 2, 3, 6, and 7. For the 1st and 2nd POMs, the coefficients a_1 and a_2 are quasi-periodic. This is confirmed in Fig. 10 that shows the result on DFT of a_j. Because the peaks (1.10 Hz and 1.30 Hz) in the DFT of a_1 and a_2 are consistent with those on ω_8 and ω_{10} in Fig. 3, the 1st and 2nd POMs identify the two-frequency swings in generators 8 and 10, respectively. On the other hand, the 3rd POM has the peak at 0.35 Hz in Fig. 10. Note that the peak at 1.10 Hz does not appear in Fig. 10 except for a_1 and a_2. Since the coherent group of generators has the dominant frequencies 0.35 Hz and 1.10 Hz, the group can be captured by the combination of the 1st, 2nd, and 3rd POMs.

Now let us summarize the difference between the obtained results with the POMs and the KMs. The POMs can have time-dependent coefficients with multiple frequencies (see Fig. 10). On the other hand, the KMs contain single frequencies by construction. Thus the KMs can capture the coherent group of generators as a superposition of distinct, single-frequency modes. Here the POD is based on energy contained in the swings. In this simulation, since the energy of the coherent group is not dominant in the swings, the POMs are not effective for directly identifying the coherent group. On the other hand, the KMs can identify the coherent group not depending on its containing energy.

IV. Application to the IEEE Reliability Test System-1996

We apply the computation of KM to analyze short-term swing dynamics in the IEEE Reliability Test System-1996 (RTS-96). The topology for RTS-96 is presented in Fig. 4 of [30]. The test system consists of three areas (Area 1 to 3) and contains the 33 generation buses (99 synchronous machines), the 40 load buses, and AC transmission lines. The original RTS-96 can include one DC transmission line, but here we do not use it for simplicity of the current analysis. Most of the buses have constant active and reactive power loads. The details of the test system, such as bus data, generator data, branch data, and system dynamic data, are available in [30]. The purpose of the application is to demonstrate that the KM analysis can identify coherent swings of synchronous machines in a large test system.

We simulate coupled swing dynamics of 96 synchronous machines following the sequence of one three-phase fault and line trip in Area 1. The details of simulation setting are given in Appendix B. Fig. 11 shows one example of time responses of rotor speed deviations ω_i for the 96 machines. The notation in the figure, e.g. U020(101), describes rotor speed deviation for Unit No. 20 connected to bus 101. Since the fault happens in Area 1, swings in Area 1 (on the top of FIg. 11) become larger than those in Area 2 and 3. In this duration all the machines swing with finite amplitudes and do not show the loss of transient stability.

Now we compute the KMs for the coupled swing dynamics shown in Fig. 11. The computation is done with the Fourier-based formula (4). For computation we need to choose frequencies that are dominant in the coupled swings. DFT analysis suggests three clean peaks appear at 0.45 Hz, 1.00 Hz, and 1.75 Hz. Fig. 12 shows the distribution of amplitude coefficients A and initial phases α for KMs with the three frequencies. The plots of A and α for 0.45 Hz are clustered around the coordinate $(0.2, 0.4)$. This clearly indicates that the coherent swing with 0.45 Hz is embedded in the coupled swing dynamics shown in Fig 11. Such a coherent mode is a dynamical key for understanding global (coherent) swing instability of the whole system (see [8], [9]). Thus, by the KM analysis, we can identify coherent swings from data obtained in a large power system.

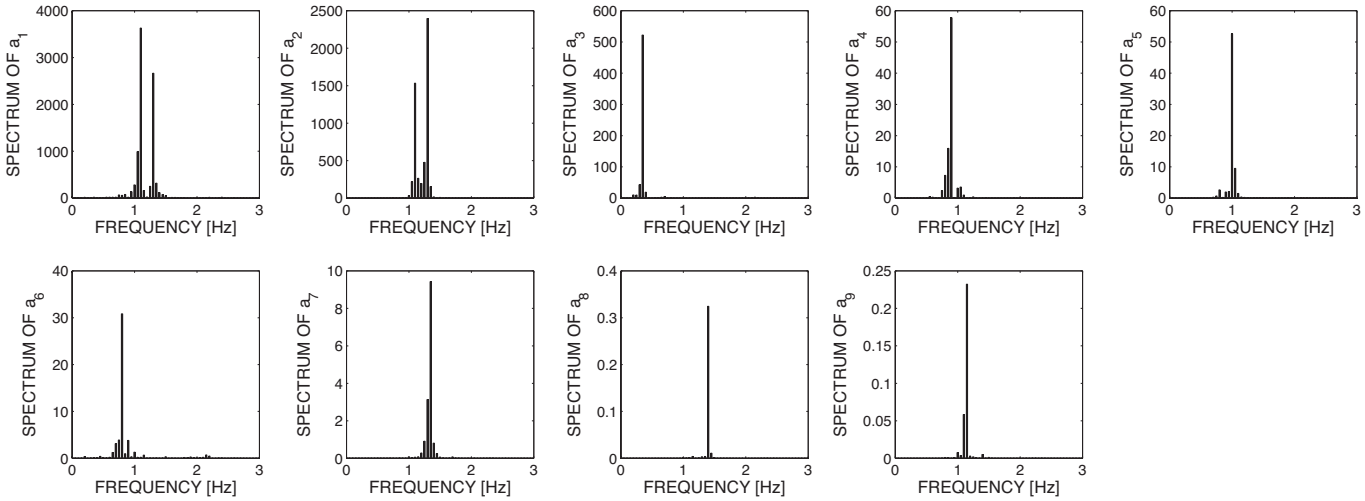

Fig. 10. Numerical discrete Fourier transform of time-varying coefficients a_j.

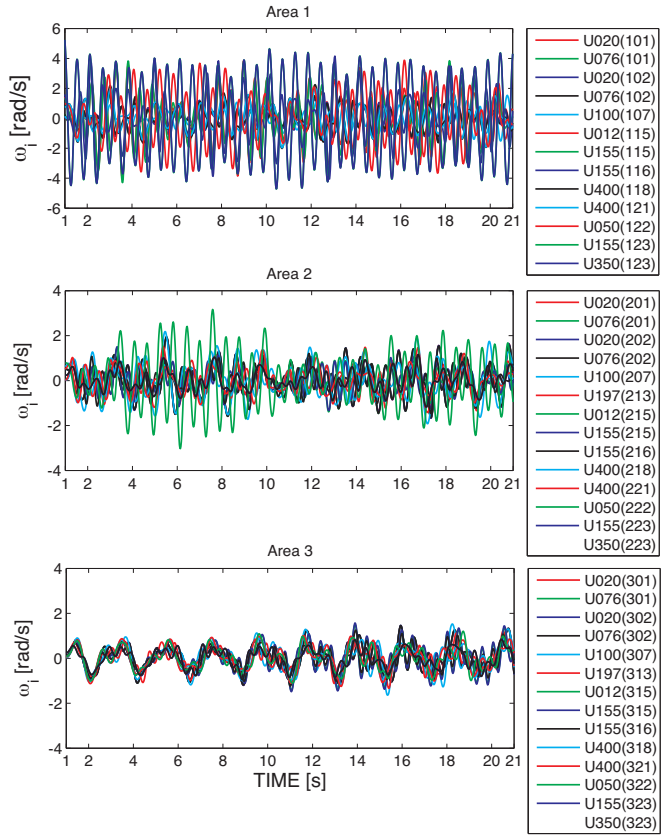

Fig. 11. Coupled swing dynamics of 96 synchronous machines in the IEEE Reliability Test System-1996. These are obtained with numerical simulation of the classical model like (8).

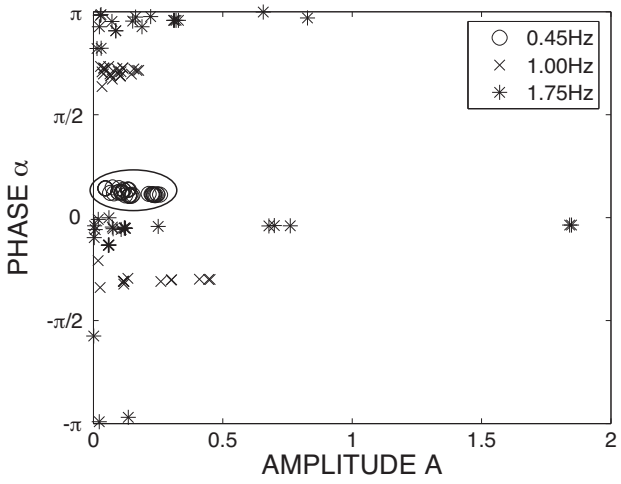

Fig. 12. Distribution of amplitude coefficients A_{ji} and initial phases α_{ji} for Koopman modes obtained from Fig. 11. These modes are computed with the Fourier-based formula (4) under $\nu = (0.45\,\mathrm{Hz})T$, $(1.00\,\mathrm{Hz})T$, and $(1.75\,\mathrm{Hz})T$.

V. Concluding Remarks

We performed modal analysis of short-term swing dynamics in the New England 39-bus test system and the IEEE Reliability Test System-1996, based on the so-called Koopman Modes (KM). Since the analysis based on the so-called Koopman operator and KM can be done on data, it does not need the access to mathematical models. We demonstrate that the KM analysis identifies single-frequency swings from transient data far from an attractor, and that the KM analysis can be used to identify coherent swings and machines accurately. Several standard techniques, which as introduced in Sec. I are the linearization [10], the time-scale separation [12]–[15], the weak coupling [18], the user-supplied grouping (described in Sec. 3.1 of [36]), have been applied to large scale power system models. All of these methods include either linear or weakly nonlinear system theory. The KM analysis is a fully nonlinear, exact technique that does not require linearization, assumptions of scale-separation, and user input. Also the KM analysis takes into account the inherent dynamics hidden in simulation outputs and data, and any clustering algorithm does not. This is explained in detail in terms of the underlying attractors in [27]. We suggest that the KM analysis provides an effective method for modal identification of transient dynamics, when

compared with the existing techniques, linearization and the Proper Orthonormal Decomposition (POD).

The coherency identified by the KM analysis is disturbance dependent because we need to select the modes which are excited by a given disturbance. On the other hand, the traditional analysis of linear global modal, which is a model-based methodology, detects all linear oscillatory modes independently of these modes being excited or not. A question now comes up: how do we find all nonlinear oscillatory modes and coherent swings? As mentioned in Sec. I, when the Koopman operator is defined for a nonlinear dynamical system, it has full information of the system, that is, all nonlinear oscillatory modes. Different basins of attraction for separate attractors will have different KMs. However, if initial conditions start in the same basin of attraction, they will have the same KM.

The KM computation can be done with two different ways: the Fourier-based formula (4) and the Arnoldi-based algorithm in Sec. II. The Fourier-based formula gives excellent accuracy when good time resolution and long time length of data are available. The Arnoldi-based algorithm is that it gives good accuracy when good special resolution and relatively short time length are available. The advantage of the Arnoldi-based algorithm can provide a new method for dynamic security assessment using the KM analysis in near-real time: see our upcoming manuscript [37].

Here, we again compare the KM decomposition with the POD. POD is essentially a linear analysis technique. As discussed in Sec. III-D, when POD is applied to a nonlinear oscillation, we often find that a POM oscillates with several frequencies. On the other hand, KM provides by definition modes oscillating with a single frequency. Also the KM analysis is known to decouple dynamics at different time scales more effectively than proper orthonormal modes [38]. Recently algorithms to compute POMs in near-real time have been discussed in literature. The Arnoldi-based algorithm to compute KMs provides a good opportunity for near real-time use, because it requires limited time length of data as discussed above.

Finally, the KM analysis gives tools for analysis and control of complex dynamics in power systems, beyond the models we considered here. In this paper, since the dynamics of power system have a finite number of discrete isolated spectral points, we used the part of quasi-periodic oscillations in (2) only for coherency identification. The remaining part of aperiodic oscillations, which is the second term on the right-hand side of (2), can be used for power system analysis with more complex dynamics, including systems with complex behaviors exhibiting chaotic behavior. Nonlinear mode interaction can be evaluated well using the KM analysis. In fact, in [37] we will consider exactly the question of mode interaction. Resonances and related dynamics such as resonance-induced chaos can be also studied using these tools.

ACKNOWLEDGEMENTS

The authors are grateful to Professor Takashi Hikihara (Kyoto University) for his constant support and fruitful suggestions. The authors are also grateful to anonymous reviewers for their critical reading of the manuscript and suggestive comments.

ERRATUM

In the published version of the paper, numerical results on initial phase information based on the KM analysis are inaccurate. Figures 4, 6, 7, and 12 have been corrected in the present version of the paper, which differs in this respect from the published one. Also, typographical errors in the published version are removed.

REFERENCES

[1] E. H. Abed and P. P. Varaiya, "Nonlinear oscillations in power systems," *Electrical Power & Energy Systems*, vol. 6, no. 1, pp. 37–43, January 1984.

[2] J. R. Winkelman, J. H. Chow, B. C. Bowler, B. Avramović, and P. V. Kokotović, "An analysis of interarea dynamics of multi-machine systems," *IEEE Transactions on Power Apparatuses and Systems*, vol. PAS-100, no. 2, pp. 754–763, February 1981.

[3] H. D. Chiang, C. W. Liu, P. P. Varaiya, F. F. Wu, and M. G. Lauby, "Chaos in a simple power system," *IEEE Transactions on Power Systems*, vol. 8, no. 4, pp. 1407–1417, November 1993.

[4] V. M. Venkatasubramanian and Y. Li, "Analysis of 1996 Western American electric blackouts," in *Proceedings of the Bulk Power System Dynamics and Control–VI*, Cortina d'Ampezzo, Italy, August 2004, pp. 685–721.

[5] A. R. Messina and V. Vittal, "Nonlinear, non-stationary analysis of interarea oscillations via Hilbert spectral analysis," *IEEE Transactions on Power Systems*, vol. 21, no. 3, pp. 1234–1241, August 2006.

[6] P. A. Parrilo, S. Lall, F. Paganini, G. C. Verghese, B. C. Lesieutre, and J. E. Marsden, "Model reduction for analysis of cascading failures in power systems," in *Proceedings of the American Control Conference*, San Diego, June 1999, pp. 4208–4212.

[7] A. R. Messina and V. Vittal, "Extraction of dynamic patterns from wide-area measurements using empirical orthogonal functions," *IEEE Transactions on Power Systems*, vol. 22, no. 2, pp. 682–692, May 2007.

[8] Y. Susuki, I. Mezić, and T. Hikihara, "Global swing instability of multimachine power systems," in *Proceedings of the 47th IEEE Conference on Decision and Control*, Cancun, Mexico, December 9–11 2008, pp. 2487–2492.

[9] ——, "Coherent swing instability of power grids," *Journal of Nonlinear Science*, (accepted).

[10] R. Podmore, "Identification of coherent generators for dynamic equivalents," *IEEE Transactions on Power Apparatus and Systems*, vol. PAS-97, no. 4, pp. 1344–1354, July/August 1978.

[11] B. Avramović, P. V. Kokotović, J. R. Winkelman, and J. H. Chow, "Area decomposition for electromechanical models of power systems," *Automatica*, vol. 16, pp. 637–648, November 1980.

[12] J. H. Chow, Ed., *Time-Scale Modeling of Dynamic Networks with Applications to Power Systems*, ser. Lecture Notes in Control and Information Sciences 46. Berlin Heidelberg: Springer-Verlag, 1982.

[13] J. H. Chow, J. Cullum, and A. Willoughby, "A sparsity-based technique for identifying slow-coherent areas in large power systems," *IEEE Transactions on Power Apparatuses and Systems*, vol. PAS-103, no. 3, pp. 463–473, March 1984.

[14] S. B. Yusof, G. J. Rogers, and R. T. H. Alden, "Slow coherency based network partitioning including load buses," *IEEE Transactions on Power Systems*, vol. 8, no. 3, pp. 1375–1382, August 1993.

[15] J. H. Chow, "New algorithms for slow coherency aggregation of large power systems," in *Systems and Control Theory for Power Systems*, J. H. Chow, P. V. Kokotović, and R. J. Thomas, Eds. New York: Springer-Verlag, 1995, pp. 95–115.

[16] S. Sastry and P. Varaiya, "Coherency for interconnected power systems," *IEEE Transactions on Automatic Control*, vol. AC-26, no. 1, pp. 218–226, February 1981.

[17] G. Troullinos and J. Dorsey, "Coherency and model reduction: State space point of view," *IEEE Transactions on Power Systems*, vol. 4, no. 3, pp. 988–995, August 1989.

[18] R. Nath, S. S. Lamba, and K. S. Prakasa Rao, "Coherency based system decomposition into study and external areas using weak coupling," *IEEE Transactions on Power Apparatus and Systems*, vol. 104, no. 6, pp. 1443–1449, June 1985.

[19] Y. Ohsawa and M. Hayashi, "Construction of power system transient stability equivalents using the Lyapunov function," *International Journal of Electronics*, vol. 50, no. 4, pp. 273–288, April 1981.

[20] M. H. Haque and A. H. M. A. Rahim, "Identification of coherent generators using energy function," *IEE Proceedings, Part C*, vol. 137, no. 4, pp. 255–260, July 1990.

[21] K. K. Anaparthi, B. Chaudhuri, N. F. Thornhill, and B. C. Pal, "Coherency identification in power systems through principle component analysis," *IEEE Transactions on Power Systems*, vol. 20, no. 3, pp. 1658–1660, August 2005.

[22] B. O. Koopman, "Hamiltonian systems and transformations in Hilbert space," *Proceedings of the National Academy of Sciences of the USA*, vol. 17, no. 5, pp. 315–318, May 1931.

[23] K. Peterson, *Ergodic Theory*. Cambridge: Cambridge University Press, 1983.

[24] A. Lasota and M. C. Mackey, *Chaos, Fractals, and Noise: Stochastic Aspects of Dynamics*. New York: Springer-Verlag, 1994.

[25] I. Mezić and A. Banaszuk, "Comparison of systems with complex behavior," *Physica D*, vol. 197, pp. 101–133, 2004.

[26] N. Wiener and A. Wintner, "Harmonic analysis and ergodic theory," *American Journal of Mathematics*, vol. 63, no. 2, pp. 415–426, April 1941.

[27] I. Mezić, "Spectral properties of dynamical systems, model reduction and decompositions," *Nonlinear Dynamics*, vol. 41, pp. 309–325, August 2005.

[28] C. W. Rowley, I. Mezić, S. Bagheri, P. Schlatter, and D. S. Henningson, "Spectral analysis of nonlinear flows," *Journal of Fluid Mechanics*, vol. 641, pp. 115–127, 2009.

[29] M. A. Pai, *Energy Function Analysis for Power System Stability*. Kluwer Academic Pub., 1989.

[30] The IEEE Reliability Test System - 1996, "A report prepared by the reliability test system task force of the application of probability methods subcommittee," *IEEE Transactions on Power Systems*, vol. 14, no. 3, pp. 1010–1020, August 1999.

[31] A. G. Phadke, "Synchronized phasor measurement in power systems," *IEEE Computer Applications in Power*, vol. 6, no. 2, pp. 10–15, April 1993.

[32] Y. Susuki and I. Mezić, "Nonlinear Koopman modes of coupled swing dynamics and coherency identification," in *2010 IEEE Power & Energy Society General Meeting*, Minneapolis, United States, July 25–29 2010.

[33] P. Kundur, *Power System Stability and Control*. McGraw-Hill, 1994.

[34] P. Holmes, J. L. Lumley, and G. Berkooz, *Turbulence, Coherent Structures, Dynamical Systems, and Symmetry*. Cambridge University Press, 1996.

[35] B. F. Feeny and B. Kappagantu, "On the physical interpretation of proper orthogonal modes in vibrations," *Journal of Sound and Vibration*, vol. 211, no. 4, pp. 607–616, 1998.

[36] W. W. Price, J. H. Chow, A. W. Hargrave, B. J. Hurysz, and P. M. Hirsch, "Large-scale system testing of a power system dynamic equivalencing program," *IEEE Transactions on Power Systems*, vol. 13, no. 3, pp. 768–773, August 1998.

[37] Y. Susuki and I. Mezić, "Nonlinear Koopman modes and a precursor to power system swing instabilities," submitted for possible publication.

[38] C. W. Rowley, I. Mezić, S. Bagheri, P. Schlatter, and D. S. Henningson, "Reduced-order models for flow control: Balanced models and Koopman modes," in *7th IUTAM Symposium on Laminar-Turbulent Transition*, Stockholm, Sweden, June 23–26 2009.

APPENDIX A
IMPLEMENTATION OF STEP (1) IN ALGORITHM

Because of $\boldsymbol{r} \perp \mathrm{span}\{\boldsymbol{g}(\boldsymbol{x}_0), \ldots, \boldsymbol{g}(\boldsymbol{x}_{N-1})\}$ we can write (5) as follows:

$$0 \;=\; \boldsymbol{g}(\boldsymbol{x}_i)^{\mathrm{T}}\boldsymbol{r} \;=\; \boldsymbol{g}(\boldsymbol{x}_i)^{\mathrm{T}}\boldsymbol{g}(\boldsymbol{x}_N) - \sum_{j=0}^{N-1} c_i \boldsymbol{g}(\boldsymbol{x}_i)^{\mathrm{T}}\boldsymbol{g}(\boldsymbol{x}_j),$$

where $i = 0, \ldots, N-1$. The matrix $\mathsf{A} = \{A_{ij}\} \in \mathbb{R}^{N\times N}$ is defined as

$$A_{ij} \;=\; \boldsymbol{g}(\boldsymbol{x}_i)^{\mathrm{T}}\boldsymbol{g}(\boldsymbol{x}_j).$$

Here, because A has at most rank $p \ll N$ in this paper, we cannot determine a unique minimizer $\boldsymbol{c} = \{c_i\} \in \mathbb{R}^N$ of the norm $||\mathsf{A}\boldsymbol{c} - \boldsymbol{b}||$ where

$$\boldsymbol{b} \;=\; \{\boldsymbol{g}(\boldsymbol{x}_i)^{\mathrm{T}}\boldsymbol{g}(\boldsymbol{x}_N)\}.$$

In this paper we obtain one solution to minimize the norm using the Moore-Penrose pseudo-inverse matrix $\mathsf{A}^\dagger$ of A. The matrix is computed with the function `pinv` in MATLAB. The solution corresponds to $\mathsf{A}^\dagger\boldsymbol{b}$.

APPENDIX B
SIMULATION SETTING FOR THE IEEE RELIABILITY TEST SYSTEM-1996

In the same way as the New England test system, we use the classical model for simulation of the IEEE Reliability Test System-1996 (RTS-96). Assume that bus 113 is the infinite bus in order to explicitly represent the outside of the system. Then the three generators connected to bus 113 are ignored in the simulation. The classical model for 96 synchronous machines in the RTS-96 is

$$\left.\begin{aligned} \frac{\mathrm{d}\delta_i}{\mathrm{d}t} &= \omega_i, \\ \frac{H_i}{\pi f_{\mathrm{b}}}\frac{\mathrm{d}\omega_i}{\mathrm{d}t} &= P_{\mathrm{m}i} - G_{ii}E_i^2 \\ &\quad - \sum_{j=0, j\neq i}^{96} E_i E_j \left\{G_{ij}\cos(\delta_i - \delta_j) + B_{ij}\sin(\delta_i - \delta_j)\right\}, \end{aligned}\right\} \quad (10)$$

where the integer label $i = 1, \ldots, 96$ denotes machine i. The variable δ_i is the angular position of rotor in machine i with respect to the infinite bus and is in radians [rad]. The variable ω_i is the deviation of rotor speed in generator i relative to system angular frequency $2\pi f_{\mathrm{b}} = 2\pi \times (60\,\mathrm{Hz})$ and is in radians per second [rad/s]. We set the variable δ_0 to a constant for the infinite bus. The parameters f_{b}, H_i, $P_{\mathrm{m}i}$, E_i, G_{ii}, G_{ij}, and B_{ij} are the same as in (8).

The setting of numerical simulation to obtain the simulation output in Fig. 11 is as follows. The voltage E_i and the initial condition $(\delta_i(0), \omega_i(0) = 0)$ for generator i are fixed using power flow computation. The inertia constant H_i is the same as in [30]. For synchronous condensers we use $H = 5\,\mathrm{s}$ and $x_d = 0$ for simplicity of the current analysis. The elements G_{ii}, G_{ij}, and B_{ij} are calculated using the data in [30] and the result of power flow computation. We use the following fault condition: each generator operates at a steady condition at $t = 0\,\mathrm{s}$. Then a three-phase fault happens at bus 123 (in Area 1) at $t = 1\,\mathrm{s} - 5/(60\,\mathrm{Hz}) = 11/12\,\mathrm{s}$, and line A21 trips at $t = 1\,\mathrm{s}$. The fault duration is 5 cycles of a 60-Hz sine wave. The fault is simulated by adding a small impedance $(10^{-7}\mathrm{j})$ between bus 123 and the ground.